ISSN 1063-7729, Astronomy Reports, 2011, Vol. 55, No. 11, pp. 1038–1050. © Pleiades Publishing, Ltd., 2011.
Original Russian Text © M.V. Eselevich, V.G. Eselevich, 2011, published in Astronomicheskii Zhurnal, 2011, Vol. 88, No. 11, pp. 1124–1136.

Some Properties of the Development of the Perturbed Zone and Shock Preceding a Coronal Mass Ejection

M. V. Eselevich* **and V. G. Eselevich**

Institute of Solar–Terrestrial Physics, Siberian Branch, Russian Academy of Sciences, Irkutsk, Russia

Received March 10, 2011; in final form, April 11, 2011

Abstract—SOHO/LASCO C2 and C3 data have been used to carry out a detailed study of the perturbed zone and shock that form as a coronal mass ejection (CME) moves away from the Sun, as a result of its interaction with the ambient solar wind. The event of January 4, 2002 is used as an example. The perturbed zone is most extensive along the direction of propagation of the CME, decreases away from this direction, and reaches its minimum values perpendicular to this direction. The mass of the perturbed zone is $\geq$0.1 of the total mass of the CME. The condition for the formation of a shock preceding the CME (in the direction of propagation of the CME) is $V - V_{SW} > V_A$, where V, V_{SW}, and V_A are the CME, solar wind, and Alfvén velocities, respectively. Perpendicular to the CME axis, at distances of ≈ 4–$6R_\odot$ from the center of the Sun, the condition for the formation of shock is $V/2 > V_A$.

DOI: 10.1134/S1063772911110023

1. INTRODUCTION

It is becoming more and more obvious that the dynamics of coronal mass ejections (CMEs), and especially the formation of a shock preceding a CME, cannot be fully analyzed without introducing the concept of a "perturbed zone" and studying its properties in detail [1]. Invoking this concept has proven to be very promising, since it has opened a real path to identifying the shocks preceding CMEs when such shocks have formed. Studies of the conditions in the perturbed zone as a function of the CME velocity relative to the ambient solar wind (SW), $u = V - V_{SW}$ (V is the measured CME velocity and V_{SW} the velocity of the unperturbed SW, both relative to the Sun), based on white-light images from the SOHO/LASCO C2 and C3 coronographs have shown the following [2]:

• when u is below a critical velocity $u_{\rm cr}$, the perturbed zone preceding the CME is elongated in the direction of propagation, and is filled with MHD oscillations and plasma flows reflected from the CME;

• when u is greater than $u_{\rm cr}$, the formation of a discontinuity is observed in the leading part of the perturbed zone in radial distributions of the difference brightness; since u_C is close to the local magnetoacoustic speed, which is approximately equal to the coronal Alfvén speed, the formation of such a discontinuity when u_C is exceeded can be identified with the formation of a shock.

Two complementary approaches to analyzing the observational data have been used to demonstrate that the observed discontinuity in the brightness distributions is indeed a shock front, and not the frontal structure of the CME moving behind the shock [3]:

(1) The conditions in the perturbed zones preceding various CMEs with various velocities u were analyzed. For CMEs whose velocities exceeded the critical speed $u_{\rm cr}$, a discontinuity corresponding to a shock front was detected in the leading part of the perturbed zone, which itself fell off fairly smoothly with distance.

(2) The evolution of the perturbed zone and formation of a shock was analyzed for individual CMEs in the frames of their frontal structures, as the CME speeds u made a transition through the critical speed $u_{\rm C}$.

Specialized studies have confirmed the correctness of measuring the width of the shock front preceding a CME δ_F using Mark 4 and LASCO C2 data [3].

Based on these studies, it was concluded that, at distances from the solar center $1.2R_\odot < R < 6R_\odot$ ($R_\odot$ is the solar radius), the width of the shock front δ_F increases with R, remaining comparable to the mean-free path for protons $\lambda_{\rm p}$, testifying to a collisional mechanism for the dissipation of energy in the shock front. At distances $R \geq 10$–$15R_\odot$, a new discontinuity with width $\delta_F^* \ll \lambda_{\rm p}$ forms in the leading part of the collisional shock front. The measured width δ_F^* remains constant with distance (within the errors), and corresponds to the spatial resolution

*E-mail: mesel@iszf.irk.ru

of LASCO C3 ($\approx 0.12R_\odot$) or STEREO/COR2 ($\approx 0.03R_\odot$), depending on the data used. This means that the true width of the discontinuity is much smaller than the measured widths (it is unresolved in the images), and this structure could be associated with a collisionless shock. This conclusion is in agreement with the results of [4]: discontinuities in the brightness distribution with minimum widths $\delta_F^* \approx 0.1$–$0.2R_\odot$ were observed in front of 13 selected CMEs with velocities above 1500 km/s at distances of $R > 6$–$10R_\odot$, which were likewise interpreted as fronts of collisionless shocks.

Studies of possible mechanisms for the formation of shocks preceding CMEs at distances $R > 10R_\odot$ were carried out in [5]. The dependence of the Alfvén Mach number M_A on the shock strength ρ_2/ρ_1 (ρ_1 and ρ_2 are the densities of the plasma ahead of and behind the front) was compared with the results of ideal MHD computations for 10 shocks with speeds $\approx$800–2500 km/s at distances 10–$30R_\odot$. These comparisons showed that the effective adiabatic index γ characterizing the processes inside the front are mainly in the range from 2 to 5/3. This corresponds to an effective number of degrees of freedom for the motion from two to three. The analogous dependence $M_A(\rho_2/\rho_1)$ was also constructed for leading near-Earth and interplanetary collisionless shocks in [5]. This supported the idea that the studied discontinuities preceding CMEs at distances $R \geq 10$–$15R_\odot$ were indeed collisionless shocks.

The aim of our current study is to investigate the properties of the perturbed zone, obtain a comparative estimate of its mass, and analyze the conditions for shock formation, not only in a limited region in the direction of propagation of a CME, but also in an arbitrary direction.

2. DATA AND ANALYSIS METHOD

We used coronal images obtained with the SOHO/LASCO C2 and C3 [6] coronographs for our analysis. These data were in the form of difference brightnesses, $\Delta P = P(t) - P(t_0)$, where $P(t)$ is the brightness of the corona at time t, corresponding to the event considered, and $P(t_0)$ is the unperturbed brightness at a specified time t_0, chosen to be well before the event. This approach excluded background brightness associated with the stationary distribution of plasma in the corona. The difference brightness was used to investigate the dynamics of the CME, perturbed zone, and preceding shock. We used contour representations of the difference brightness to select events and carry out a general analysis of these events. The contour levels were selected based on the character of the event and the distance being considered. When conducting quantitative analyses, we used radial profiles of the difference brightness $\Delta P(R)$ constructed from the center of the Sun along a specified position angle PA, as well as non-radial difference-brightness profiles $\Delta P(r)$ constructed from a point in a direction deemed to be of interest. The difference in notation underscores the fact that the distance R is measured from the center of the Sun, and r from some other point in the image. Further, all distances in the figures are expressed in units of $R_\odot$. In most of the events, the difference-brightness profiles do not form "thin" cross sections occupying a single pixel, and were averaged over a finite angle (1°–2°). This averaging was done to improve the signal-to-noise ratio in the distributions.

3. ANALYSIS OF FEATURES IN THE PERTURBED ZONE PRECEDING THE CME

3.1. Basis for Selecting CMEs for the Analysis

It is currently considered to be well established that a large portion of CMEs with large angular sizes ($d > 30°$–$50°$) are comprised of magnetic flux ropes or tubes filled with plasma. According to [7], the orientation of the axis of the CME flux rope approximately coincides with the orientation of the neutral line (NL) of the magnetic field in the region of the CME source on the Sun, or of a filament along the NL. The angle between the NL and the North–South direction on the Sun is denoted γ. "Limb" CMEs arising at longitudes $\Phi > 60°$ with large angles $\gamma > 45°$ have the simplest appearance in white-light observations, and are convenient for studies of their three-part structures: the frontal structure (FS), region of reduced density (cavity), and bright core [8]. This is the type of CME that was observed on January 4, 2002 (at ≈09:05; here and below, all times are UT), which was selected for our analysis of the dynamics of the perturbed zone and shock. The coordinates where it originated on the Sun are ≈N25E72; $\gamma \approx 62°$. According to the catalog http://cdaw.gsfc.nasa.gov/CME_list/, the velocity of the CME at $R \approx 5$–$6R_\odot$ was ≈900 km/s. This means that its speed relative to the ambient SW was $u = V - V_{SW} \approx 750$ km/s, close to the local Alfvén speed, $V_A \approx 700$ km/s. In this case, we expect a minimum size for the perturbed zone preceding the CME.

3.2. Analysis of the $\Delta P(r)$ Distribution in the Frame of the CME Frontal Structure

Figure 1 shows the difference brightness as contour plots for three successive times, corresponding to the motion of this CME in the LASCO C2

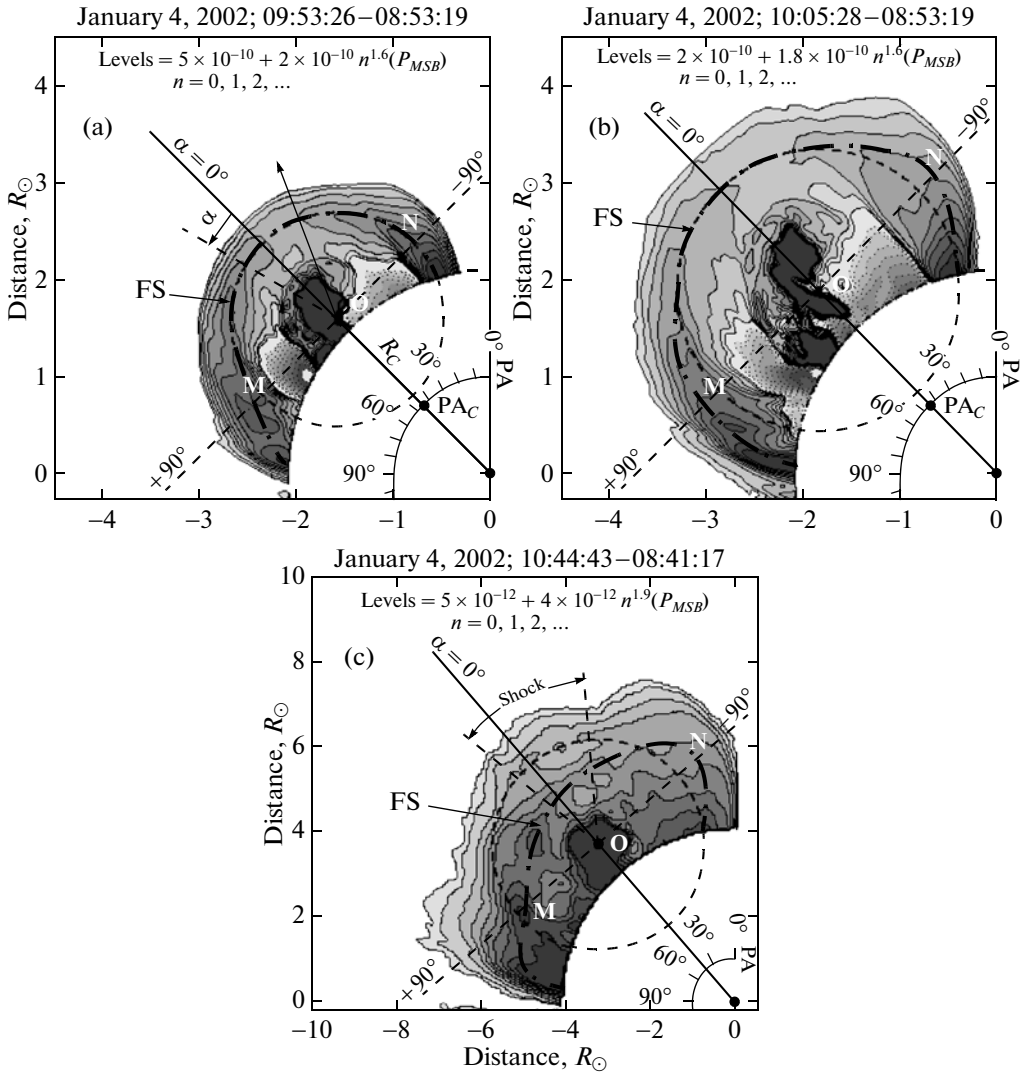

Fig. 1. Images of the CME of January 4, 2002 shown as contour plots of the difference brightness for three successive times. Expressions for the difference-brightness levels for the shaded contours in units of the mean solar brightness (P_{MSB}) are given. The scale of image (c) constructed from LASCO C3 data differs from the scale for images (a) and (b), which were constructed from LASCO C2 data.

(Figs. 1a, 1b) and C3 (Fig. 1c) fields of view. Expressions giving the contour levels in units of the mean brightness of the solar disk, P_{MSB}, are shown in each image.

The frontal structure (FS) of the CME, shown in Fig. 1 by a bold, dot-dashed curve, is drawn through the local brightness maxima, which are easily distinguished in the contours. At the initial time (Fig. 1a), the frontal structure is close to circular (dashed circle). The shape of the frontal structure changes at the later times, although a circle that nearly coincides with the frontal structure can be drawn in these cases as well. The positions of these circles that are close to the frontal structure were used to make ties to the CME at the corresponding times. The center of the frontal structure at the point O is determined by the position angle PA_C and the distance R_C from the center of the Sun. The direction along PA_C roughly coincides with the axis for the CME motion (shown by the solid line in Figs. 1a–1c). The difference-brightness profiles $\Delta P(r)$ were constructed from the center of the frontal structure for various angles α, measured counter-clockwise from the CME axis (Fig. 1a).

For convenience in the analysis, the difference-brightness profiles $\Delta P(r)$ were constructed in the frame of the frontal structure, as follows [3].

(1) Each profile $\Delta P(r)$ was normalized to the corresponding maximum difference brightness in the vicinity of the frontal structure.

(2) Each profile $\Delta P(r)$ (except for the first in time) was shifted along the r axis by an amount Δr, such that the positions of the frontal structure in all the profiles coincided. In the direction of motion of the CME (PA $\approx 46°$), $\Delta r = \Delta R$.

3.3. Characteristics of the Perturbed Zone as a Function of α

Figure 2 shows contour plots of the difference brightness $\Delta P(r)$ constructed in this way for three successive times (filled circles, hollow circles, filled triangles) for eight directions: $\alpha = -90°$, $-50°$, $-40°$, $-6°$, $0°$, $+30°$, $+50°$, $+90°$. The position of the frontal structure is marked by "FS" and a vertical arrow. The region with horizontal shading in the plots shows the leading boundary of the frontal structure, corresponding to a current sheet. The width of the current sheet δ_I (mraked in the first panel) was taken to be twice the width of the brightness jump at half the peak of the frontal structure.

At the first time 09:53:26 (filled circles), the width of the current sheet $\delta_I \approx 0.2R_\odot$ is essentially independent of α. At the following time 10:05:28 (hollow circles), the smallest width $\delta_I \approx 0.2R_\odot$ is observed only at the maximum angles $|\alpha| = 90°$. The width δ_I grows as $|\alpha|$ decreases, becoming $\delta_I \approx 1R_\odot$ when $\alpha \approx 0°$. This is in agreement with the conclusions of [3] that the development of the perturbed zone as a result of the interaction of the CME with the ambient SW leads to an increase in the observed width δ_I.

The perturbed zone is shown by the region with vertical shading in Fig. 2. In all directions, the left-hand boundary of the perturbed zone was taken to be the position of the leading boundary of the frontal structure at half its height at time 09:53:26 (shown by dark circles). A broadening of the profile due to strong interaction of the CME with the unperturbed SW, leading to a growth in the perturbed zone, is observed at small $|\alpha|$. The perturbed zone is formed most efficiently in the direction of motion of the CME ($\alpha \approx 0°$). The shock is marked in the leading part of the perturbed zone by the cross-hatching in Figs. 2a, 2b, and 2e.

A similar pattern for the variation of the perturbed zone can be traced in the images in Fig. 1. At the first time, 09:53:26 (Fig. 1a), the position of the frontal structure at all α (bold dot-dashed curve) nearly precisely corresponds to the circle shown by the dashed curve. Only for directions $\alpha \approx +70-+110°$ does the position of the frontal structure deviate slightly from an outward circular arc. At the next time, 10:05:28 (Fig. 1b), this deviation is greater, and appreciable departures from circularity also appear at $\alpha \approx -60...-110°$, i.e., on the opposite side of the CME. Since the interaction of the CME with the unperturbed SW is more efficient in the direction of its motion than perpendicular to this direction, there is a "compression" of the frontal structure in the direction of motion of the CME, so that it gradually takes on an elliptical form (Figs. 1b, 1c). By 10:44:43 (Fig. 1c), a discontinuity in the difference-brightness distribution forms in directions $-40° \leq \alpha \leq +8°$ in the leading part of the perturbed zone, which, according to the interpretation of [2, 3], represents a shock.

3.4. Estimates of the Mass of the CME and Perturbed Zone

An important characteristic of the interaction of the CME with the unperturbed SW is the mass of the perturbed zone, M_{PZ}, compared to the mass of the CME, $M_{\rm CME}$. We can estimate these two masses using the white-light difference-brightness images. Only the brightness of the CME and associated perturbed zone is present in these difference images, since the background coronal brightness has been subtracted. Knowing the brightness due to scattering of the photospheric radiation on a single electron in the corona [9], we can use the difference brightness to obtain the total number of electrons and the mass of matter in the corona, assuming 1.97×10^{-24} g of matter per scattering electron (this assumes that the matter consists of 90% H and 10% He). Since the real distribution of matter along the line of sight is not known, we assume for these estimates that all the matter is concentrated in the plane of the sky, this will provide a lower limit for the masses. The total mass is calculated by suming the difference brightnesses within a selected area of the image.

The mass estimate was made using difference images obtained with the LASCO C2 and C3 coronographs. For the summation, we used the sector of the images located between position angles 0 and 90°, where most of the CME propagation occurred. We used distances of $2.1R_\odot$ and $6R_\odot$ from the solar center for the lower and upper boundaries of this region in the C2 images, and distances of $4.1R_\odot$ and $20R_\odot$ for the C3 images. Figure 3a shows a LASCO C3 image of the CME at 10:44:43 in the form of contours of the difference brightness, which shows the sector within which the mass was calculated. The lower boundary of the summation region is shown by the solid curve, and the upper boundary is beyond the edge of the image. We used the region of the sector beyond a distance R_Z (dashed curve in Fig. 3a) to calculate the mass of the perturbed zone. R_Z was selected at each time to be the distance of the maximum of the frontal structure in the direction of motion of the CME ($\alpha \approx 0°$) plus half the width of the current sheet, $\delta_I/2 \approx 0.15R_\odot$, measured at the initial time, 09:53:26

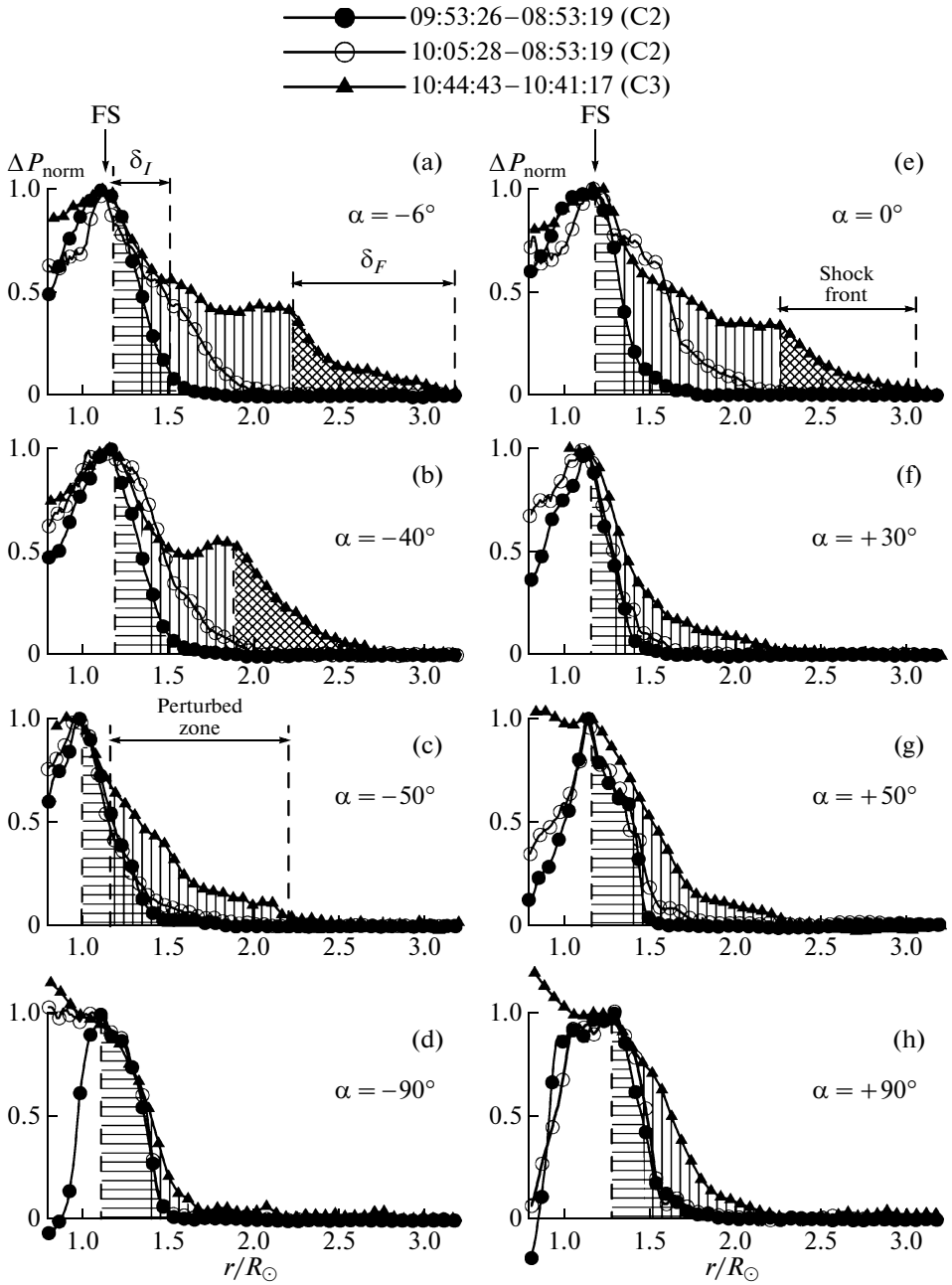

Fig. 2. Profiles of the difference brightness $\Delta P(r)$, constructed as a function of the distance r from the center of the CME in the frame of the frontal structure. The left-hand and right-hand panels show profiles constructed along negative and positive angles α. The module of α increases from 0 to 90° from top to bottom. The profiles shown by different symbols correspond to different times on January 4, 2002.

(Fig. 2e). This addition is appreciable at early times, when the extent of the perturbed zone is small.

The circles in Fig. 3b show the total mass of the CME derived from the C2 (filled) and C3 (hollow) images. As the CME moves, only part of it lies in the field of view of the C2 coronograph. Initially, part of the CME lies below the eclipsing disk, and the measured masses are therefore below the maximum mass; the measured masses then grow as an increasing fraction of the CME lies in the field of view. Further, the C2 masses decrease as a larger fraction of the CME lies beyond the coronograph field of view. A similar pattern of variations of the measured mass is obtained for the C3 data. However, in this case, there is a time interval covering two to three images (about one hour) when virtually the entire CME is

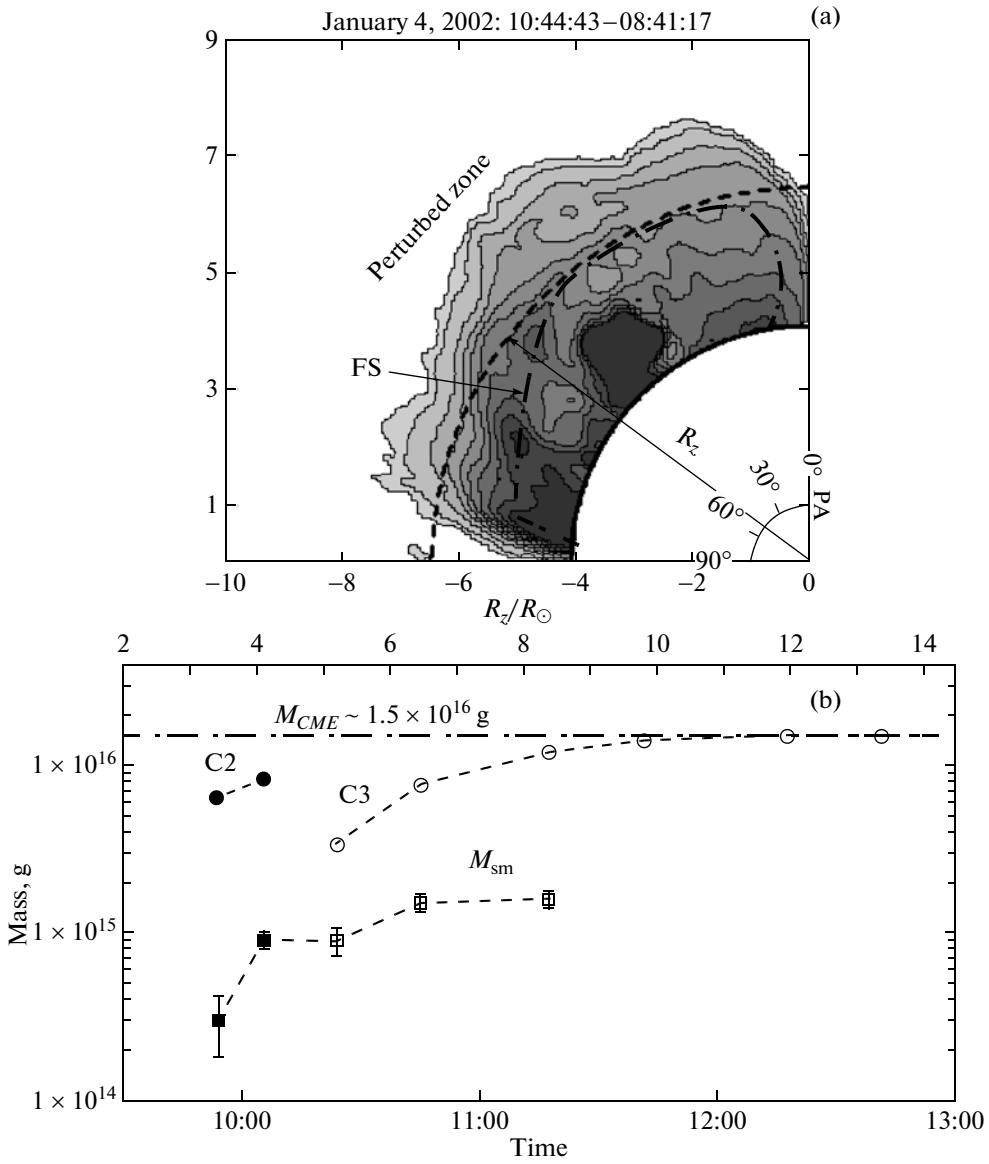

Fig. 3. (a) Sector of an image of the CME at 10:44:43, used to calculate the mass of the CME of January 4, 2004. The section of the sector beyond a distance R_Z from the solar center (its inner boundary is shown by the dashed curve) was used to calculate the mass of the perturbed zone. (b) Mass of the CME (circles) and the perturbed zone (squares) measured at various times based on the LASCO C2 and C3 data (filled and hollow symbols, respectively). The distance R_Z beyond which the mass of the perturbed zone was determined is plotted on the upper horizontal axis. The variation of the measured mass of the CME is due to its passage in the field of view of the coronographs; the estimated total mass of the CME is 1.5×10^16 g (horizontal dash-dotted line).

located in the field of view of the coronograph (more precisely, within the summation region, $4.1–20R_\odot$). During this interval, the mass reaches its maximum value and remains virtually constant. This maximum mass, $M_{\rm CME} \approx 1.5 \times 10^{16}$ g, is an estimate for the total mass of the CME (horizontal dot-dashed line in Fig. 3b).

The mass of the perturbed zone M_{PZ} beyond a distance R_Z from the solar center was measured in the same way (an axis marked with this distance is shown on the top in Fig. 3b). The derived masses are shown by the squares in Fig. 3b. The perturbed zone is always located within the coronograph field of view, since it corresponds to the most forward part of the CME. Therefore, variations in the measured masses of the perturbed zone reflect real variations. As the CME moves outward, the mass of the perturbed zone increases, reaching 10% of the total mass $M_{\rm CME}$.

To estimate the uncertainty of these measurements, we calculated the mass using difference images obtained at two times when the CME was not yet in the coronograph fields of view: 09:05:24–08:53:19 for C2 and 09:17:26–08:41:16 for C3. The resulting mass reflects background variations associated with the residual passage of previous CMEs. These values are shown as errors for the estimates of the mass of the perturbed zone in Fig. 3b.

4. ANALYSIS OF CONDITIONS FOR THE FORMATION OF A SHOCK AHEAD OF A CME

4.1. Conditions for Shock Formation as a Function of α

During the interaction of the moving CME with the amabient plasma that leads to the formation of the shock, the velocity component normal to the surface of the frontal structure relative to the unperturbed SW is important. The velocities of individual parts of the frontal structure are comprised of the radial velocity of its center and its expansion velocity relative to the center $V_{exp}/2$, where V_{exp} is the total expansion velocity of the CME. According to [10], $V_{exp} \approx V$, where V is the radial velocity of the leading part of the CME (i.e., where $\alpha = 0°$). Thus, if the normal velocity component of the frontal structure in the direction of motion of the CME is V, this velocity is approximately a factor of two lower ($\approx V/2$) in lateral directions ($\alpha = \pm 90°$).

The motion of the CME occurs against the background of the predominantly radial motion of the SW at the velocity V_{SW}. Consequently, the normal component of the relative velocity along $\alpha \approx 0°$ will be $V - V_{SW}$, and this component in the directions $\alpha \approx \pm 90°$ will be $\approx V/2$, since the speed of the SW is then tangent to the surface of the frontal structure, and does not influence the formation of the shock. For the CME of January 4, 2002, we expect the optimal conditions for shock formation ahead of the CME at $R \approx 4–6R_\odot$ at angles $\alpha \approx 0°$, since, according to [11], $V_{SW} \sim 100$ km/s at these distances, and the velocity of the leading part of the CME is $V \sim 700 - 800$ km/s; i.e., the condition $V - V_{SW} > V/2$ is satisfied. Further, we consider this question in more detail.

4.2. Formation of a Shock Ahead of the CME

Let us consider shock formation ahead of the CME for three directions: along the propagation axis of the CME ($|\alpha| \leq 10°$) and perpendicular to this axis ($\alpha \approx \pm 90°$).

4.2.1. $|\alpha| \leq 10°$. The formation of a shock (cross-hatched region) at the leading edge of the perturbed zone (region with vertical shading) is visible in the direction of motion of the CME, $\mathrm{PA_C} = 43°–46°$ (Fig. 4a) in the difference-brightness profiles constructed in the frame of the frontal structure (Fig. 4a). At a distance of $R \approx 7.7R_\odot$, the width of the shock front is $\delta_F \approx 0.8R_\odot$ (filled triangles in Fig. 4a; $\Delta R \approx 3.2R_\odot$). The width δ_F is determined as the scale over which ΔP decreases from its maximum value immediately behind the front to one-tenth of this value.

Let us consider the dynamics of the shock front at distances $R > 6R_\odot$. Figures 4b–4e show profiles of the difference brightness $\Delta P(R)$ constructed along the direction of motion of the CME for successive times, based on the C3 data. These represent a continuation of the plots in Fig. 4a to larger distances from the Sun, and are plotted as functions of the distance R from the solar center. (The difference of PA_C from its values at $R < 6R_\odot$ is due to the small nonradiality of the CME propagation.) The hollow circles show difference-brightness profiles constructed for time 09:41:21, just before the appearance of the CME. These distributions serve as estimates of the noise levels at various distances, which become stronger with distance from the Sun; i.e., the signal-to-noise level worsens with distance. As in Figs. 2 and 4a, the shock front is shown in the difference-brightness profiles by the region of cross-hatching. The character of the variations of the shock-front width δ_F with distance (filled circles in Fig. 5a) corresponds to the dependence $\delta_F(R)$ obtained earlier in [3, 13] (solid curve in Fig. 5a). Since δ_F is comparable to the mean-free path of the protons λ_p (calculated values for two coronal temperatures, 10^6 K and 2×10^6 K, are shown by the dashed curves in Fig. 5a), the shock is apparently collisional.

The formation of a new discontinuity is observed at distances $< R \approx 19R_\odot$ in the leading part of the front (gray shading in Figs. 4e–4g, where the spatial scale is more extended than in Fig. 4d). The measured width of the discontinuity, $\delta_F^* \approx 0.1–0.2R_\odot$ is an order of magnitude smaller than the mean-free path, and remains constant with distance (hollow circles in Fig. 5a). The formation of a discontinuity with width $\delta_F^* \ll \lambda_\mathrm{p}$ at distances $10R_\odot \leq R \leq 30R_\odot$ was reported earlier in [3]. Here, too, δ_F^* was $\approx 0.1–0.2R_\odot$ within the uncertainties, and was independent of distance (horizontal dash-dotted line in Fig. 5a). The spatial resolution of C3 is $K \approx 0.12R_\odot$, roughly equal to the observed width of the discontinuity, δ_F^*. Thus, the true scale for the discontinuity could be appreciably smaller than the observed width, since it is simply not resolved in coronal images. This, together with the fact that δ_F^* remains constant with distance,

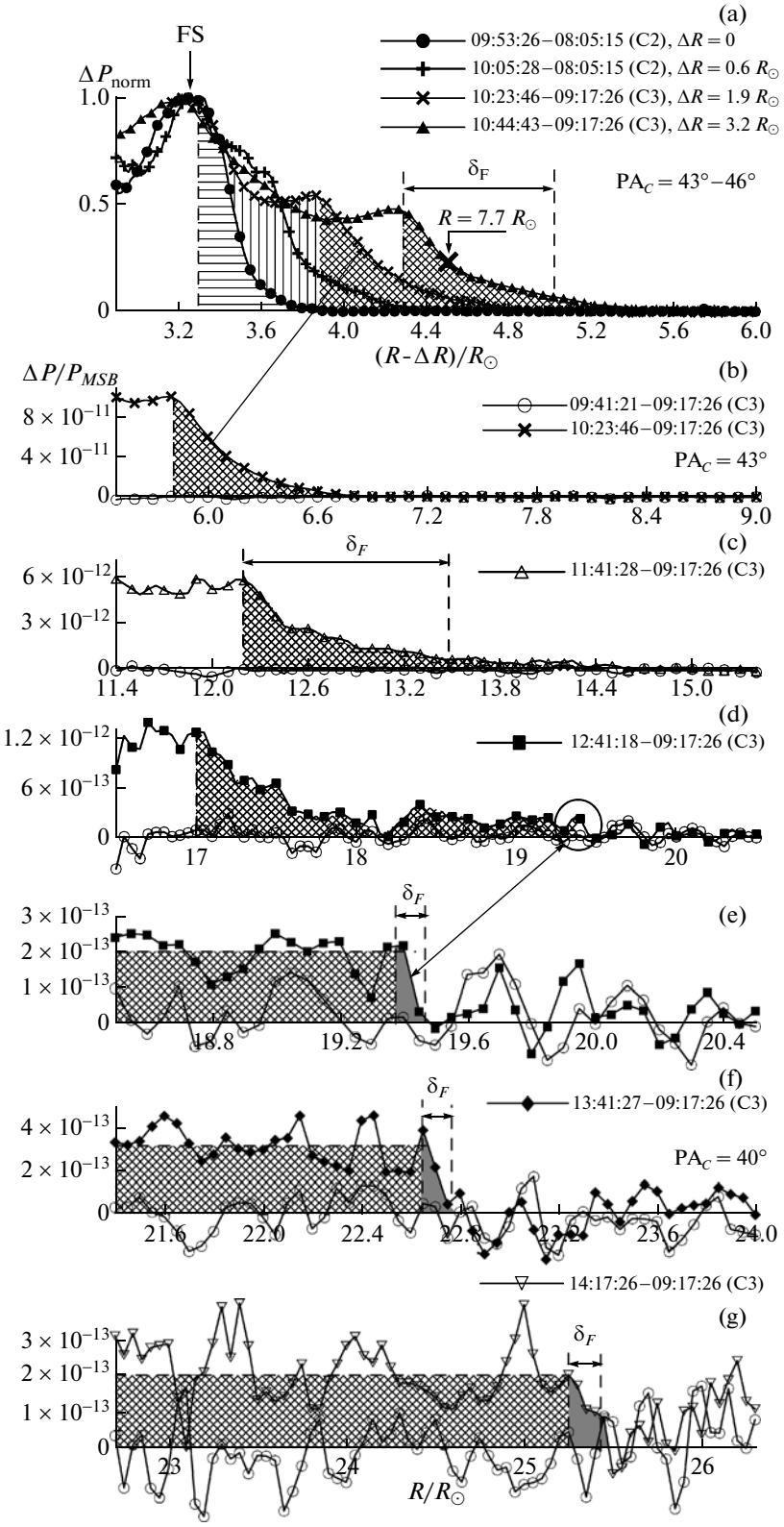

Fig. 4. Profiles of the difference brightness ΔP constructed approximately along the direction of propagation of the CME (PA = 43°–46° or $\alpha \approx 0°$) at successive times on January 4, 2002: (a) in the frame of the frontal structure and (b)–(g) relative to the center of the Sun. The profile in panel (b) repeats the corresponding profile in (a) in the other frame (shown by the ×'s). The profile in (e) repeats the corresponding profile in (d) on a more expanded scale (shown by filled squares). The modest variations of the main direction of motion of the CME, PA_C, are associated with non-radiality of the CME propagation.

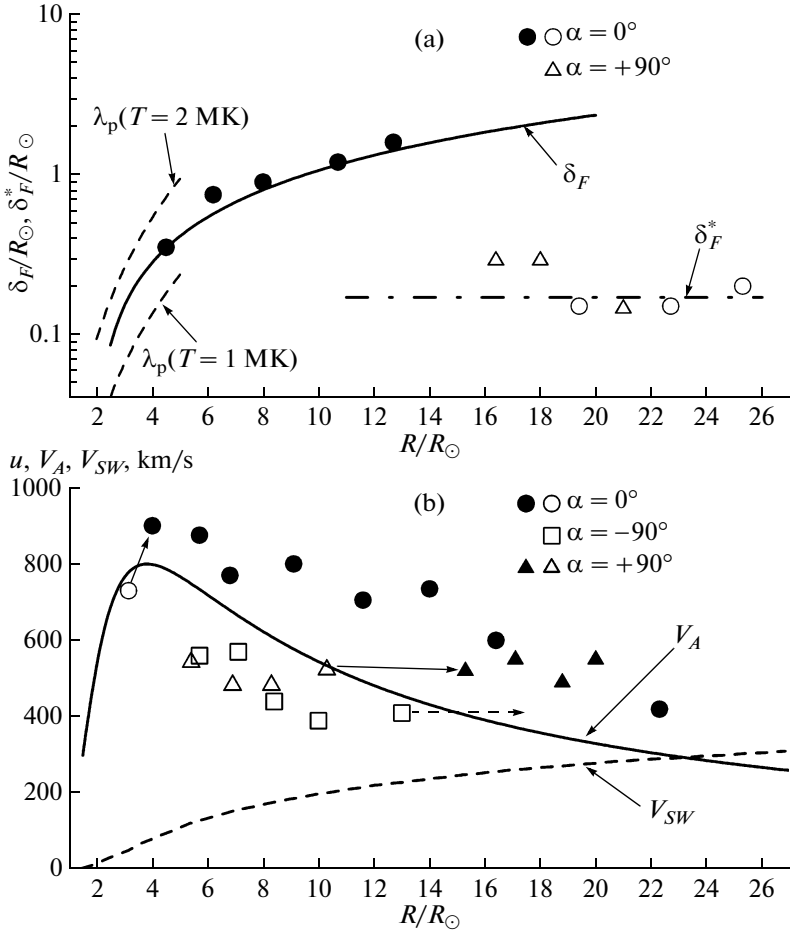

Fig. 5. Dependences of various quantities on the distance R from the solar center calculated for the CME of January 4, 2002. (a) Width of the front of a collisional (δ_F; filled symbols) and collisionless (δ_F^*; hollow symbols) shock excited by the CME; the dashed curves are the calculated mean-free paths for protons λ_p in the streamer belt for the two temperatures 10^6 and 2×10^6 K; the solid curve and dot-dashed line show the experimental dependences $\delta_F(R)$ and $\delta_F^*(R)$ from [3], respectively. (b) Velocities u of the leading edge of the perturbed zone of the CME (hollow symbols) and of the shock (filled symbols) relative to the ambient SW for angles $\alpha \approx 0°$ (circles), $\alpha \approx -90°$ (squares), and $\alpha \approx +90°$ (triangles); the dashed curve shows the velocity of the quasi-stationary, slow SW V_{SW} in the streamer belt from [11]; the solid curve shows the calculated Alfvén velocity in the streamer belt from [12].

testifies that this discontinuity is a collisionless shock, whose front width is not resolved, so that the measured width is determined by the spatial resolution of the C3 coronograph.

According to the studies [3, 13] based on more than 30 CMEs, the criterion for the formation of a shock front ahead of a CME is that the relative velocity $u = V - V_{SW}$ exceed the local Alfvén velocity $V_A(R)$, calculated in [12]. The circles in Fig. 5b show u as a function of R for the CME considered here together with the $V_A(R)$ curve from [12] (solid curve). The one hollow circle corresponds to two times when the perturbed zone without a shock was observed ahead of the CME. The velocity was determined from the position of the leading boundary of the frontal structure. The filled circles show the relative velocity, determined from the position of the shock front after its formation. All the filled circles are located above the $V_A(R)$ curve ($u > V_A$), while the hollow circle is below this curve ($u < V_A$). The formation of the shock (the transition from the hollow to the filled circles as the $V_A(R)$ curve is crossed) occurs near $R \approx 4R_\odot$ (shown by the arrow in Fig. 5b).

4.2.2. $\alpha = -90°$. Figure 6a shows difference-brightness profiles for five successive times in the frame of the frontal structure for $\alpha = -90°$. The position of the frontal structure along $\alpha = -90°$ is marked by the vertical arrow labeled "FS" in Fig. 6a (this point is denoted by N in Fig. 1). The region of horizontal shading denotes the current sheet at the leading boundary of the frontal structure, and the region of vertical shading the perturbed zone for the

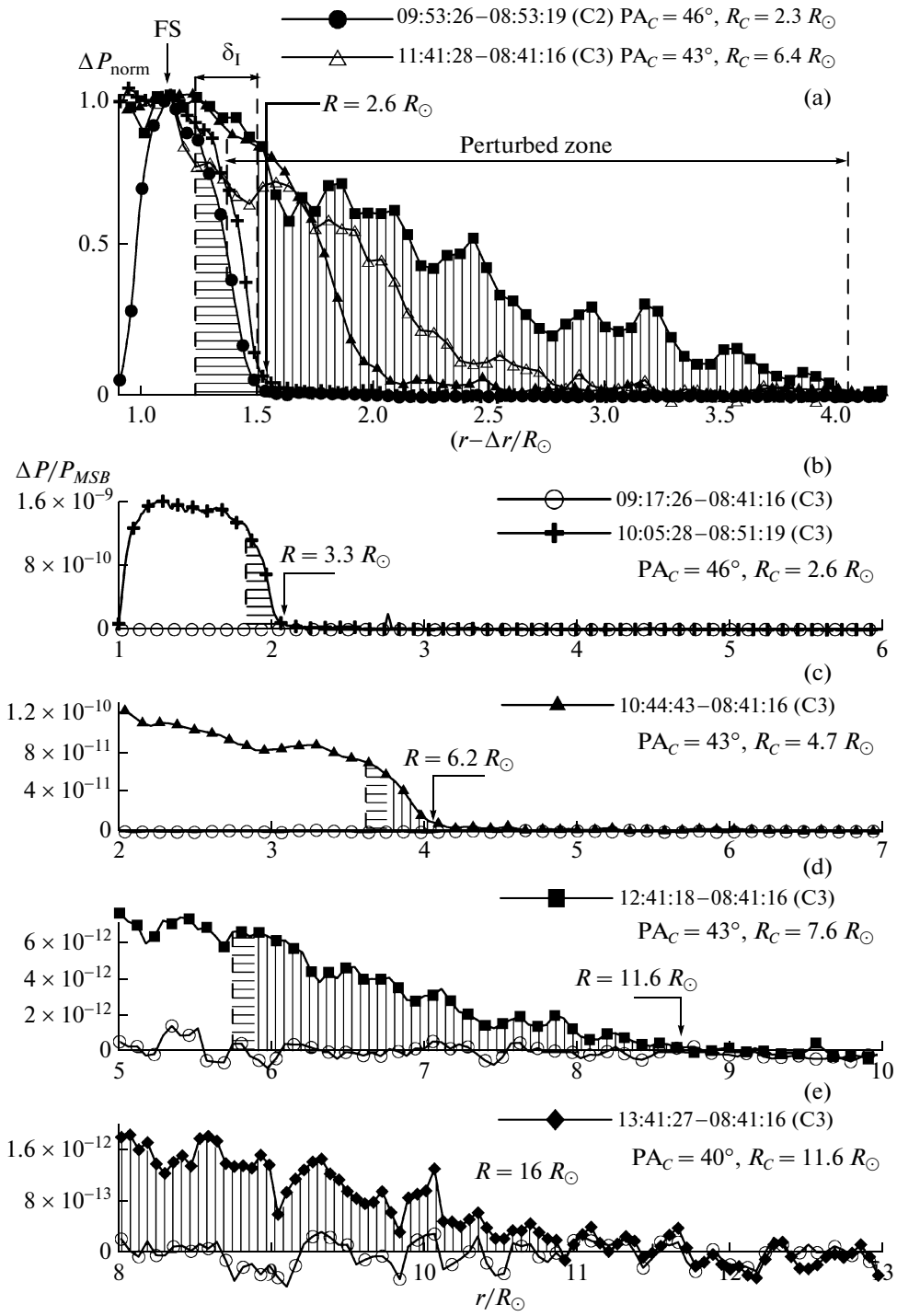

Fig. 6. Difference-brightness profiles analogous to those in Fig. 4 but along $\alpha \approx -90°$. The profiles in (b) shown by the pluses and in (c) shown by filled triangles repeat the corresponding profiles in (a) in the other frame.

last time, 12:41:18 (squares). Figure 6a shows that, as the CME moves, the perturbed zone preceding its frontal structure develops—its amplitude and size are increased. By 12:41:18, it forms a region of decreasing difference brightness $\approx 2.5 R_\odot$ in size. The perturbed zone is inhomogeneous and is filled with oscillations, probably of a magnetohydrodynamical nature, with a characteristic wavelength of $\sim 0.5 R_\odot$. There is no shock. Let us estimate the speed of the CME in this direction.

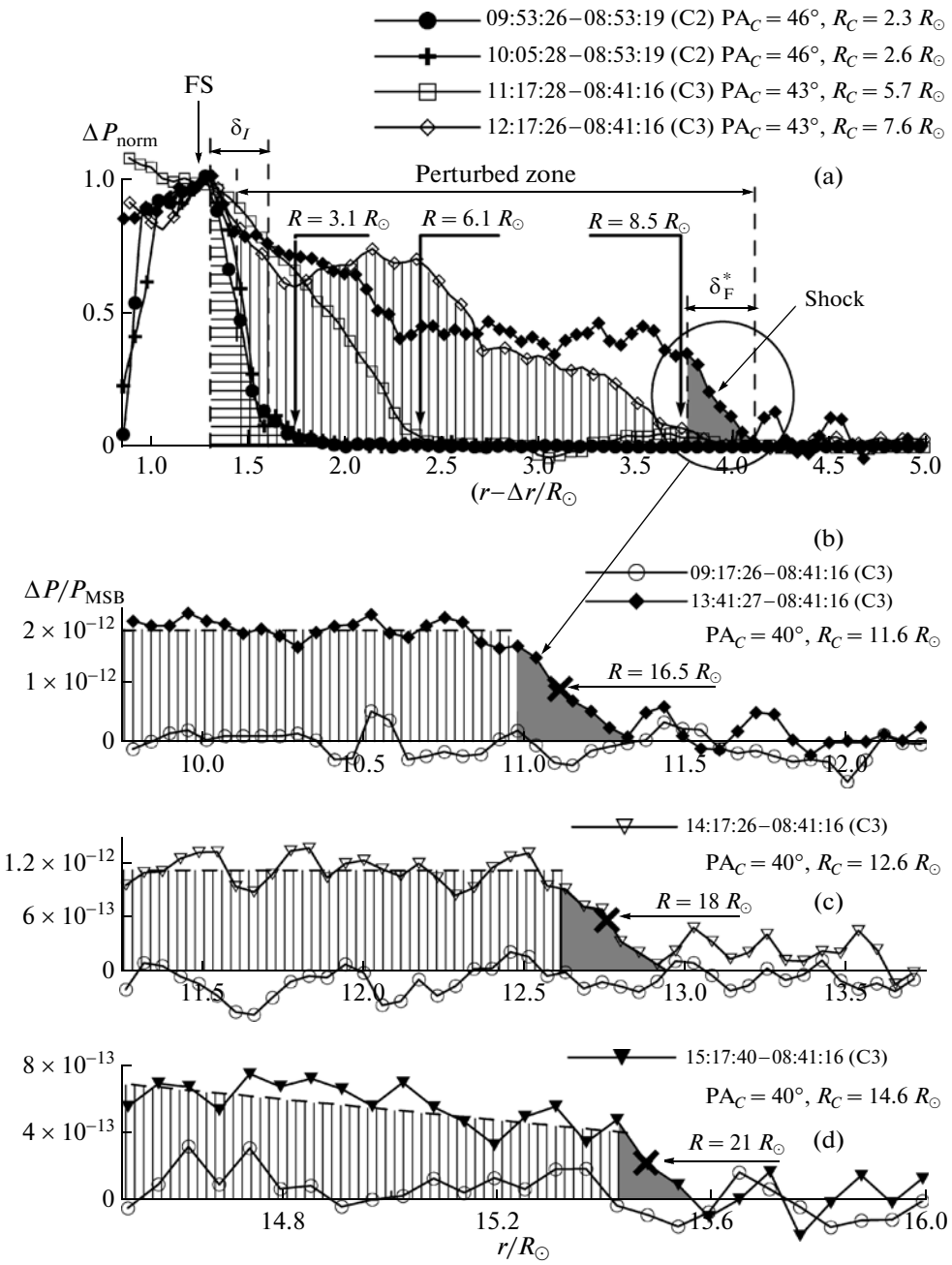

Fig. 7. Difference-brightness profiles analogous to those in Fig. 4 for $\alpha \approx +90°$. The profile in (b) shown by the filled diamonds repeats the corresponding profile in (a) in the other frame.

Figures 6b–6e show distributions of the difference brightness $\Delta P(r)$ for successive times for $\alpha = -90°$ as a function of the distance r from the center of the frontal structure. The position of the center of the frontal structure (distance from the center of the Sun R_C and position angle PA$_C$) is presented for each time in Fig. 6.

At large distances, the frontal structure is no longer visible as a well defined maximum in the difference-brightness profiles. Here, the perturbed zone is determined by the part of the profile that is furthest from the center of the frontal structure, for which a monotonic drop in the difference brightness down to zero is observed (region of vertical shading in the profiles). The size of the current sheet at the boundary of the frontal structure (region of horizontal shading) is shown in the profiles based on its size at the first time, 09:53:26 (Fig. 6a).

The distance from the solar center to any point along a profile in the directions $|\alpha| = 90°$ is obvi-

ously $R = (R_C^2 + r^2)^{0.5}$, where r is the distance to the considered point from the center of the frontal structure. The distances R from the solar center of the most distant points in the profiles $\Delta P(r)$ are marked by vertical arrows with headings in Figs. 6b–6e. (In Fig. 6a, $R = 2.6R_\odot$ is indicated for time 09:53:26.) The velocity along $\alpha = -90°$ was determined for these points, using the distance r from the center of the frontal structure. Since the velocity V_{SW} of the unperturbed SW is directed nearly radially, the relative velocity of the CME along $\alpha = -90°$ is equal to the measured velocity, whose dependence on R is shown in Fig. 5b by the hollow squares. All the derived velocities are located below the curve $V_A(R)$. This explains why the shock has not yet formed in the direction $\alpha = -90°$ at these distances. We infer from Fig. 5b that the formation of the shock front should also be observed at distances $R \geq 15R_\odot$, but this is hindered by the high noise level at these distances.

4.2.3. $\alpha = +90°$. The position of the frontal structure along $\alpha = +90°$ is marked by the letter M in Fig. 1. Figure 7a shows difference-brightness profiles for five successive times in the frame of the point M for $\alpha = +90°$. Similar to the previous figures, the horizontal-shaded region shows the current sheet at the boundary of the frontal structure at time 09:53:26 (filled circles), and the vertical-shaded region the perturbed zone at time 12:17:26 (hollow diamonds). Figure 7a shows that, as for the direction $\alpha = -90°$, the perturbed zone ahead of the frontal structure is strengthened as the CME moves. By 12:17:26 (hollow diamonds in Fig. 7a), it forms a region of decreasing difference brightness ahead of the frontal structure $\approx 2–2.5R_\odot$ in size. The leading parts of the perturbed zone are marked in Fig. 7a by the vertical arrows with indicated distances from the solar center R. We determined the speed of this region along $\alpha = +90°$ using these points, shown in Fig. 5b by the hollow triangles. These points in Fig. 5b lie below the curve $V_A(R)$. The characteristic size of oscillations of the difference brightness in the perturbed zone is $\sim 1R_\odot$ at time 12:17:26 (hollow diamonds in Fig. 7a). By the following time, 13:41:27 (filled diamonds), a brightness discontinuity or shock with width $\delta_F^* \approx 0.3R_\odot \ll \lambda_p$ is observed in the leading part of this zone (shaded gray).

Figures 7b–7d present distributions of the difference brightness $\Delta P(r)$ along $\alpha = +90°$ as a function of the distance r from the center of the frontal structure, beginning from 13:41:27. Figure 7b shows that the shock is first detected at $R \approx 16.5R_\odot$ from the center of the Sun. The shock is stably present at subsequent times. The minimum measured front width is $\delta_F^* \approx 0.15R_\odot$ (hollow triangles in Fig. 5a). The speed of the front was determined from the observed change in its position (the point at half its amplitude, shown by the X in Figs. 7b–7d), shown by the filled triangles in Fig. 5b. This speed was close to the relative speed of the CME u along $\alpha = 0°$ at distances $R \approx 15–20R_\odot$.

5. CONCLUSION

Generalizing our results for three different directions relative to the center of the CME frontal structure in the event considered leads to the following conclusions.

1. With increasing distance from the Sun, interaction with the SW leads to the appearance of a perturbed zone around the CME. The size of this zone grows rapidly in the direction of motion of the CME, and more slowly in the lateral directions. This is in agreement with results obtained earlier for other events.

2. The formation of a shock begins at $R \geq 4R_\odot$ in the direction of propagation of the CME ($\alpha = 0°$) and at $R \geq 8R_\odot$ along the direction $\alpha = +90°$, while the formation of a shock is not observed out to $R \approx 16R_\odot$ in the direction $\alpha = -90°$. Thus, as the CME moves away from the Sun, the shock first forms in a narrow region in the direction of motion of the CME, and only later at larger angles relative to this direction. This explains the fact that the first reliable measurements of a shock were obtained within a narrow region near the direction of motion of the corresponding CME [2].

3. The conditions for the formation of a shock ahead of a CME along the directions $\alpha \approx 0°$ and $\pm 90°$ relative to the motion of the CME are determined by the local inequalities $u(\alpha \approx 0°) \approx V - V_{SW} \geq V_A$ and $u(\alpha \approx \pm 90°) \approx V/2 \geq V_A$, where V, V_{SW}, and V_A are the CME, SW, and Alfvén velocities, respectively.

4. The width of the shock front at distances $R \leq 6R_\odot$ grows roughly as the local mean-free path for protons ($\delta_F \sim \lambda_p$). At distances $R > 6R_\odot$, the formation of a sharp front with size $\delta_F^* \approx 0.1–0.2R_\odot$ is observed. This agrees with earlier conclusions based on studies of about 30 CMEs with various velocities [3]. A new result we have obtained is that these conclusions are also valid for the lateral directions relative to the motion of the CME.

ACKNOWLEDGMENTS

This work was supported by the Russian Foundation for Basic Research (projects 09-02-00165-a and 10-02-00607-a). The SOHO/LASCO data used were obtained by a consortium formed by the US Naval Research Laboratory, the Max Planck Institute for Aeronomy (Germany), the Institute for Space Astrophysics (France), and Birmingham University (United Kingdom).

REFERENCES

1. M. V. Eselevich and V. G. Eselevich, Astron. Rep. **51**, 947 (2007).
2. M. V. Eselevich and V. G. Eselevich, Geophys. Res. Lett. **35**, L22105 (2008).
3. M. V. Eselevich, Astron. Rep. **54**, 173 (2010).
4. V. Ontiveros and A. Vourlidas, Astrophys. J. **693**, 267 (2009).
5. M. V. Eselevich and V. G. Eselevich, Astron. Rep. **55**, 359 (2011).
6. G. E. Brueckner, R. A. Howard, M. J. Koomen, et al., Solar Phys. **162**, 357 (1995).
7. H. Cremades and V. Bothmer, Astron. Astrophys. **422**, 307 (2004).
8. R. M. E. Illing and A. J. Hundhausen, J. Geophys. Res. **91**, 10 951 (1986).
9. D. E. Billings, *A Guide to the Solar Corona* (Academic Press, New York, 1966).
10. R. Schwenn, A. dal Lago, E. Huttunen, et al., Ann. Geophys. **23**, 1033 (2005).
11. Y.-M. Wang, N. R. Sheeley, D. G. Socker, et al., J. Geophys. Res. **105**, 25 133 (2000).
12. G. Mann, H. Aurass, A. Klassen, et al., in *Plasma Dynamics and Diagnostics in the Solar Transition Region and Corona, Proceedings of the 8th SOHO Workshop,* ESA Publs. No. SP-446, 477 (1999).
13. M. V. Eselevich, V. G. Eselevich, Astron. Rep. **53**, 173 (2009).

Translated by D. Gabuzda